Characteristics of spectral-hole burning in Tm^{3+}:YAG based on the perturbation theory*

Zhang Shi-Yu(张世宇)[a)b)], Ma Xiu-Rong(马秀荣)[a)b)†], Zhang Shuang-Gen(张双根)[b)], Chen-Lei(陈 雷)[a)b)], Wang Xia-Yang(王夏洋)[a)b)], Mu Kuan-Lin(穆宽林)[a)b)], and Wang Song(王 松)[a)b)]

[a)] *Engineering Research Center on Communication Devices (Ministry of Education), School of Computer and Communication Engineering, Tianjin University of Technology, Tianjin* 300384, *China*

[b)] *Tianjin Key Laboratory of Film Electronic and Communication Device, School of Electronic Information Engineering, Tianjin University of Technology, Tianjin* 300384, *China*

(Received 20 August 2013; revised manuscript received 10 December 2013; published online 20 April 2014)

In this paper, the physical mechanism of the interaction between electromagnetic wave and spectral-hole burning crystal material is investigated in detail. In the small signal regime, a perturbation theory model is used to analyze the mechanism of spectral-hole burning. By solving the Liouville equation, three-order perturbation results are obtained. From the theoretic analysis, spectral-hole burning can be interpreted as a photon echo of the zero-order diffraction echo when the first optical pulse and the second optical pulse are overlapped in time. According to the model, the spectral-hole width is dependent on the chirp rate of the reading laser. When the chirp rate is slow with respect to the spectral features of interest, the spectral hole is closely mapped into time domain. For a fast chirp rate, distortions are observed. The results follow Maxwell–Bloch model and they are also in good agreement with the experimental results.

Keywords: perturbation theory, spectral-hole burning, photon echo

PACS: 03.50.De, 42.62.Fi, 06.30.Ft, 63.20.–e **DOI:** 10.1088/1674-1056/23/6/060304

1. Introduction

Spectral-hole burning (SHB) crystal material has been found to have a wide variety of applications, such as radio frequency (RF) signal processing,[1,2] optical memory,[3] quantum memories,[4] generating arbitrary wave form,[5,6] measuring optical frequency stability,[7] etc. Spectral-hole burning is a process by which spectrally varying absorption features are formed in material that contains inhomogeneously broadened absorbers.

A spectral hole in an inhomogeneously broadened medium can be created by a single optical pulse. A theoretical model based on Maxwell–Bloch equations for the study of spectral-hole burning growth has been presented.[8] Bloch equations describe the rotation of Bloch vector, representing the population inversion and the polarization of a two-level atom, driven by an electric field. When a single optical pulse excites resonant absorbers from the ground state to the excited state, a change appears in the steady-state absorption at the resonant frequency — the spectral hole.

When two collinear optical pulses are separated in time, where one is a replica of the other, a spectral grating in an inhomogeneously broadened medium will be created. For readout of a spectral grating, the interaction of the chirped field with the spectral grating generates a delayed photon echo signal. In 1985, Mitsunaga and Brewer[9] proposed a generalized perturbation theory for an inhomogeneously broadened two-level quantum system interacting with an optical field of arbitrary pulse shape.[10] This has the advantage that all coherence phenomena can be treated together in one theory to any desired order. However, their study did not give much insight into spectral-hole burning growth. Following Mitsunaga and Brewer,[9] Colice *et al.*[2] used third-order perturbation theory to describe both the process of engraving spectral holes by modulating signal beams and the subsequent readout process with chirped laser. However, they did not explain in detail the relationship between spectral-hole burning and three-pulse photon echo.

In the present paper, we bridge the gap between spectral-hole burning and three-pulse photon echo based on perturbation theory. Solving the Liouville equation, three-order perturbation results are obtained. According to the theoretical result, when the first optical pulse and the second optical pulse are overlapped in time where one is a replica of the other, a spectral grating with just one fringe will be created. When the frequency-chirped reading laser diffracts out of the newly created spectral grating, the detector will sense the transmitted signal, which is the spectral-hole. We also call the transmitted signal the zero order diffraction of photon echo.[3] According to this model, we can put the study of the spectral hole burning and the photon echo to a unified theoretical model. The theoretical analysis indicates that the spectral-hole width is dependent on the chirp rate of the reading laser. We also experimentally demonstrate that in Tm^{3+}:YAG within cryogenic

*Project supported by the Special Funds for Scientific and Technological Innovation Projects, Tianjin, China (Grant No. 10FDZDGX00400).

†Corresponding author. E-mail: maxiurong@gmail.com

© 2014 Chinese Physical Society and IOP Publishing Ltd

temperature the spectral-hole width is dependent on chirp rate of the reading laser. Our numerical simulation and experimental results are in good agreement with each other, they are also consistent with the Maxwell–Bloch model.

2. Analysis of spectral-hole burning by perturbation theory

A SHB crystal is a rare-earth ion-doped, inhomogeneously broadened optical absorber, which can be modeled as a two-level system.[2,11] When cryogenically cooled, it has a sub-MHz homogeneous linewidth $\Delta\Gamma_{\rm H}$ and a GHz inhomogeneous bandwidth $\Delta\Gamma_{\rm I}$[9] as shown in Fig. 1. Each homogeneous frequency can be individually accessed using properly tuned narrow laser line excitation. When a monochromatic laser source (called a pump beam) at frequency $\omega_{\rm P}$ with intensity $I_{\rm P}$ irradiates a cryogenically cooled SHB crystal, ions at a frequency $\omega_{\rm p}$ that is nearly resonant with the pump beam absorb the photons and are then excited from their ground states, yielding a spectral hole in the crystal's absorption band.[2,10] Consequently, the corresponding absorption coefficient $\alpha(\omega_{\rm P},z)$ is reduced.

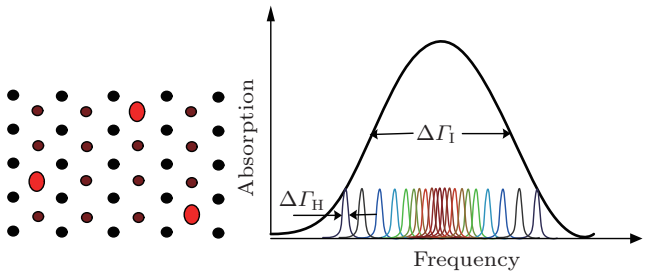


Fig. 1. (color online) Homogeneous linewidth $\Delta\Gamma_{\rm H}$ and inhomogeneous linewidth $\Delta\Gamma_{\rm I}$.

In a steady state, we can use the Maxwell equation of motion to write an expression for the complex absorption that depends on the strength of incident beam:[12]

$$\mathrm{d}E(z,t)/\mathrm{d}z = \mathrm{i}(K/2\varepsilon)P(z,t) = -\alpha(\omega_{\rm p},z)E(z,t), \qquad (1)$$

where ε is the permittivity of the host medium, $E(z,t) = \varepsilon(t)\exp[\mathrm{i}(\omega\cdot t - K\cdot t)]$, with $\varepsilon(t)$ being the envelope, and riding on a carrier at ω, K is the wave vector, $P(z,t)$ is the macroscopic polarization and $P(z,t) = 2\mu_{12}\rho_{12}(z,t)$,[2] μ_{12} is the electric dipole moment, and $\rho_{12}(z,t)$ is the off-diagonal element of the density matrix. Accordingly, the complex absorption coefficient is given as follows:

$$\begin{aligned}\alpha(\omega_{\rm p},z) &= -\mathrm{i}(K/2\varepsilon)P(z,t)/E(z,t)\\ &= -\mathrm{i}(\mu_{12}K/\varepsilon)\rho_{12}(z,t)/E(z,t). \qquad (2)\end{aligned}$$

We begin with our derivation of $\rho_{12}(z,t)$ by solving Liouville equation[10]

$$\frac{\mathrm{d}\rho}{\mathrm{d}t} = (\mathrm{i}/\hbar)\left[\rho,\hat{H}\right], \qquad (3)$$

where

$$\rho = \begin{bmatrix} \rho_{22} & \rho_{21} \\ \rho_{12} & \rho_{11} \end{bmatrix}$$

is the density matrix, $\hat{H} = \hat{H}_0 + \hat{H}_1$ is the Hamiltonian, which consists of the field-free term

$$\hat{H}_0 = \begin{pmatrix} \hbar\omega_0/2 & 0 \\ 0 & -\hbar\omega_0/2 \end{pmatrix}$$

and the field-dependent term

$$\hat{H}_1 = \begin{pmatrix} 0 & -\mu_{12}E(z,t) \\ -\mu_{12}E(z,t) & 0 \end{pmatrix},$$

$\hbar$ is the Planck constant.

According to Ref. [10], with the following initial conditions $\rho'_{12}(-\infty) = 0$ and $w(t=-\infty) = -1 = w_0$, the third order perturbative results are shown below:

$$\begin{aligned}
&w^{(0)}(t) = w_0,\\
&\rho'^{(1)}_{12}(t) = -\mathrm{i}w_0\int_{-\infty}^{t} s(t_1)\,\mathrm{e}^{-(t-t_1)/T_2}\,\mathrm{d}t_1,\\
&w^{(2)}(t) = 2\mathrm{i}^2 w_0\int_{-\infty}^{t}\mathrm{d}t_2\int_{-\infty}^{t_2}\mathrm{d}t_1[s^*(t_1)s(t_2)\\
&\quad + s(t_1)s^*(t_2)]\,\mathrm{e}^{-[(t_2-t_1)/T_2]-(t-t_2)/T_1},\\
&\rho'^{(3)}_{12}(t) = -2\mathrm{i}^3 w_0\int_{-\infty}^{t}\mathrm{d}t_3\int_{-\infty}^{t_3}\mathrm{d}t_2\int_{-\infty}^{t_2}\mathrm{d}t_1 s(t_3)\\
&\quad\times[s^*(t_1)s(t_2) + s(t_1)s^*(t_2)]\,\mathrm{e}^{-[(t-t_3+t_2-t_1)/T_2]-(t_3-t_2)/T_1},
\end{aligned}$$

where w is the population difference,

$$s(t) = -(\mu_{12}/\hbar)E(z,t)\,\mathrm{e}^{-\mathrm{i}(\omega_0-\omega)t-\mathrm{i}\omega K\cdot t},$$

T_1 is the population decay time, T_2 is the dipole dephasing time, and the time ordering is $t_1 < t_2 < t_3 < t$.

So, we can obtain the time-domain, the third-order solution for the coherent response of an inhomogeneously broadened medium to a set of incident fields,

$$\begin{aligned}\left\langle\tilde{\rho}^{(3)}_{12}(t)\right\rangle &= -\frac{2\mathrm{i}w_0\mu_{12}|\mu_{12}|^2}{\hbar^3}\int_{-\infty}^{t}\mathrm{d}t_3\\ &\quad\times\int_{-\infty}^{t_3}\mathrm{d}t_2\int_{-\infty}^{t_2}\mathrm{d}t_1 E_3(z,t_3)E_2(z,t_2)E_1^*(z,t_1)\\ &\quad\times\exp(-(t-t_3+t_2-t_1)/T_2-(t_3-t_2)/T_1)\\ &\quad\times\exp(-(t-t_1-t_2+t_3)^2/4\Delta\Gamma_{\rm I}^2). \qquad (4)\end{aligned}$$

If we assume that the Gaussian due to the inhomogeneous absorption bandwidth is wide compared with the bandwidth of the signals we are using, then the last exponential term in Eq. (4) becomes a delta function and the density matrix element responsible for polarization induced in the material is

$$\begin{aligned}\left\langle\tilde{\rho}^{(3)}_{12}(t)\right\rangle &= A\int_{-\infty}^{t}\mathrm{d}t_3\int_{-\infty}^{t_3}\mathrm{d}t_2\int_{-\infty}^{t_2}\mathrm{d}t_1 E_3(z,t_3)E_2(z,t_2)E_1^*(z,t_1)\\ &\quad\times\exp(-(t-t_3+t_2-t_1)/T_2-(t_3-t_2)/T_1)\\ &\quad\times\delta(t-t_1-t_2+t_3), \qquad (5)\end{aligned}$$

where A is the proportionality constant and

$$A = -\frac{4\mathrm{i}\sqrt{\pi}w_0\mu_{12}|\mu_{12}|^2}{(1/T_2^*)\hbar^3}$$

and we drop the spatial dependence $s(t)$.

The time-domain integrals given in Eq. (5) provide a good description of photo echoes. In order to relate to spectral-hole burning, we can apply a Fourier transform to Eq. (5) to obtain a set of frequency-domain integrals. Using the definition of the Fourier transform $E(z,t) = \int E(f)\exp(\mathrm{i}2\pi ft)\,\mathrm{d}f$, we rewrite the time-domain result in Eq. (5) as follows:

$$\begin{aligned}\langle\tilde{\rho}_{12}^{(3)}(t)\rangle = A&\int_{-\infty}^{t}\mathrm{d}t_3\int_{-\infty}^{t_3}\mathrm{d}t_2\int_{-\infty}^{t_2}\mathrm{d}t_1\\ &\times\int_{-\infty}^{\infty}\mathrm{d}f_3E_3(f_3)\exp(\mathrm{i}2\pi f_3t_3)\\ &\times\int_{-\infty}^{\infty}\mathrm{d}f_2E_2(f_2)\exp(\mathrm{i}2\pi f_2t_2)\\ &\times\int_{-\infty}^{\infty}\mathrm{d}f_1E_1^*(f_1)\exp(-\mathrm{i}2\pi f_1t_1)\\ &\times\exp[-(t-t_3+t_2-t_1)/T_2]\\ &\times\exp[-(t_3-t_2)/T_1]\delta(t_2-t_1+t_3-t).\end{aligned}\quad(6)$$

Integrating over t_1, t_2, and t_3 gives

$$\begin{aligned}\langle\tilde{\rho}_{12}^{(3)}(t)\rangle = A&\int_{-\infty}^{\infty}\mathrm{d}f_3\int_{-\infty}^{\infty}\mathrm{d}f_2\int_{-\infty}^{\infty}\mathrm{d}f_1E_3(f_3)E_2(f_2)E_1^*(f_1)\\ &\times\exp[\mathrm{i}2\pi(f_3+f_2-2f_1)t_3]\\ &\times\gamma_1(f_2-f_1)\gamma_2(f_3+f_2-2f_1),\end{aligned}\quad(7)$$

where the excited state lifetime is described by a convolution with the Lorentzian

$$\gamma_1(f_2-f_1) = \frac{1}{1/T_1+\mathrm{i}2\pi(f_2-f_1)},\quad(8)$$

and the coherence time is described by a convolution with the Lorentzian

$$\gamma_2(f_3+f_2-2f_1) = \frac{1}{2/T_2+\mathrm{i}2\pi(f_3+f_2-2f_1)}.\quad(9)$$

Equation (7) represents the causal nature of Eq. (5) more compactly and without introducing any additional approximation. The Lorentzian in Eqs. (8) and (9) fully account for the causality embodied in the time ordering of Eq. (5), since a complex Lorentzian is the Fourier transform of an exponential decay and a Heaviside step function, which embodies the time ordering. The Lorentzian in Eq. (9) has a width of $2/T_2$ rather than $1/T_2$ because the coherence time manifests itself twice, once during the interaction between $E_1^*(f_1)$ and $E_2(f_2)$, and again during the interaction between $E_3(f_3)$ and the emitted field, which is consistent with the results in Ref. [1]. This reference mentioned that the absolute limit measured hole-width is twice the homogeneous linewidth of ions.

Now, we use frequency-domain integrals to predict the spectral performance of SHB spectrum analyzers. We define the incident signals $E_1(z,t) = E_2(z,t-\Delta t)$ separated in time by delay Δt, here we drop the spatial dependence in $E(z,t)$, where $\varepsilon(t)$ is the envelope from the RF modulation and ω_0 is the optical carrier frequency. We describe the engraving process in the frequency domain by using the notation $E_1(f) = E_2(f)\cdot\mathrm{e}^{-\mathrm{j}2\pi f\cdot\Delta t}$ and substituting it into Eq. (7).

Consider a pair of beams that interfere in the crystal to write a spatial-spectral grating. However, in the experimental geometry described in the next section there is no spatial component for the grating, so spatial variation is ignored in this analysis. This can be justified by imagining that the angle between the interfering beams shrinks to zero, so the spatial grating contains just one fringe, which is described by Eq. (12). We can write the chirped beam as $E_3(z,t) = A_1\cos\left(2\pi f_3t+\kappa t^2/2\right)$, where κ is the chirp rate in Hz/s. In the frequency domain, the chirped beam is

$$E_3(f) = A_1\sqrt{2\pi/\kappa}\,\mathrm{e}^{\mathrm{i}\left[-4\pi^2(f-f_3)^2/2\kappa+\pi/4\right]}.$$

Substituting the signal fields and the chirp field into Eq. (7) yields

$$\begin{aligned}\langle\tilde{\rho}_{12}^{(3)}(t)\rangle = A&\int_{-\infty}^{\infty}\mathrm{d}f_3\int_{-\infty}^{\infty}\mathrm{d}f_2\int_{-\infty}^{\infty}\mathrm{d}f_1A_1\sqrt{2\pi/\kappa}\\ &\times\exp\{\mathrm{i}[-2\pi^2(f-f_3)^2/\kappa+\pi/4]\}E_2(f_2)E_1^*(f_1)\\ &\times\exp[(\mathrm{i}2\pi(f_3+f_2-2f_1)t)]\\ &\times\gamma_1(f_2-f_1)\gamma_2(f_3+f_2-2f_1).\end{aligned}\quad(10)$$

Because of $T_1 = 10$ ms ($\gg T_2\approx 10$ μs), we approximate the Lorentzian in Eq. (10) as $\delta(f_2-f_1)$, integrate over f_1, and rearrange the resulting integrals to obtain

$$\begin{aligned}\langle\tilde{\rho}_{12}^{(3)}(t)\rangle = A&\int_{-\infty}^{\infty}\left[\int_{-\infty}^{\infty}|E_2(f_2)|^2\,\mathrm{e}^{-\mathrm{j}2\pi f\cdot\Delta t}\gamma_2(f_3-f_2)\,\mathrm{d}f_2\right]\\ &\times A_1\sqrt{2\pi/\kappa}\,\mathrm{e}^{\mathrm{i}\left[-2\pi^2(f-f_3)^2/\kappa+\pi/4\right]}.\end{aligned}\quad(11)$$

In Eq. (11), we can find that the signal power spectrum, $|E_2(f_2)|^2$, determines the locations and depths of the spectral holes, while the Lorentzian line shape of the ionic resonances fixes the hole shapes. Spectral holes filter the incident chirp, $\exp\{\mathrm{i}[-2\pi^2(f-f_3)^2/\kappa+\pi/4]\}$, to produce the changes in the time-averaged density matrix element $\langle\tilde{\rho}_{12}^{(3)}(t)\rangle$, which determines the emitted field. Introducing a new function $H(f)$ as a shorthand for signal power spectra as recorded by the SHB crystal

$$H(f) = \int_{-\infty}^{\infty}|E_2(f_2)|^2\,\mathrm{e}^{-\mathrm{j}\omega\cdot\Delta t}\gamma_2(f_3-f_2)\,\mathrm{d}f_2.\quad(12)$$

Here, $H(f)$ acts as a transfer function, whose the shape is determined by the incident signals. In Fig. 2, $H(f)$ is analyzed in detail.

Figure 2 shows the simulation of $H(f)$ in Eq. (12). In the above analogy, SHB crystals act as programmable filters. Incident signals determine the filter shape, which changes the inhomogeneous absorption profile. From Fig. 2(a) it follows that when the first optical pulse and the second optical pulse are overlapped in time, where one is a replica of the

other, a spectral grating with just one fringe will be created. When the frequency-chirped reading laser diffracts out of the newly created spectral grating (a), the detector will sense the diffracted fields. The diffracted field, which is a transmitted signal, is the spectral-hole. We also call the transmitted signal the zero order diffraction of photon echo, which is shown in Fig. 3(a). When two collinear optical pulses are separated in time ($\Delta t = t_2 - t_1 < T_2$, T_2 is the coherence time), where one is a replica of the other, the two optical pulses interfere in the SHB crystal and write a spectral grating, which is shown in Figs. 2(b1)–2(b3). The frequency-chirped reading laser diffracts out of the spectral grating (b), and the detector will sense the transmitted field (zero-order photon echo)[3] and will transmit the first-order photon echo, which is shown in Fig. 3(b).

From Fig. 2, we can see that spectral grating changes with time interval. The time intervals of the incident signals will result in the time interval between the transmission signal and the photon echo. In addition, the photon echo intensity decreases with the increase of time interval. This happens because the macro-induction electric polarization, which is caused by the first pulse beam, decreases with the increase of the time interval.

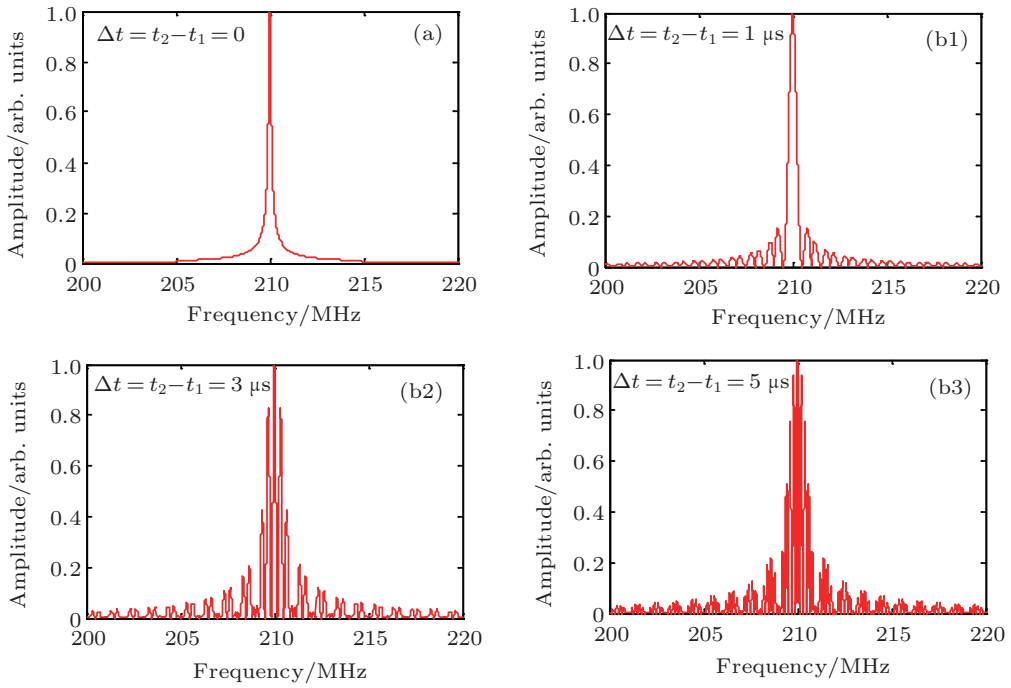


Fig. 2. (color online) Amplitude frequency characteristic curves of the varying inhomogeneous absorption profile. (a) The first pulse and the second pulse are overlapped in time, and (b) the two collinear optical pulses are separated in time (b1) $\Delta t = 1$ μs, (b2) $\Delta t = 3$ μs, (b3) $\Delta t = 5$ μs.

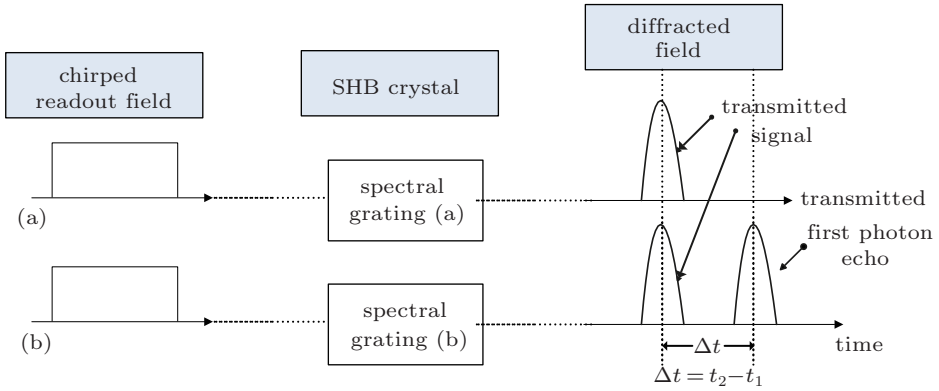


Fig. 3. Schematic diagram of chirped readout mechanisms of spectral absorption features.

Figure 3 shows the schematic illustration of chirped readout mechanisms of spectral absorption features. The left side of the schematic plot shows the input chirped field, the middle represents the medium with different spectral absorption features, and the right side shows the diffracted field. Spectral gratings (a) and (b) represent the cases of Figs. 2(a) and

2(b), respectively. For the effective mapping of the hole into a temporal intensity profile, the frequency of the chirped field should scan over the hole width Γ for a time $\delta t > 1/\Gamma$, which implies that a chirp rate $\kappa < \Gamma^2$ should be used.

To study the effect of spectral-hole width dependence on the chirp rate of the reading laser, we calculate the spectral-hole width from Eq. (11). The linear frequency-chirped laser operates on the 200 MHz∼220 MHz where amplitude $E_0 =$ 1 V, the homogeneous linewidth of the ions $\Gamma = 1$ MHz, the chirp rates $\kappa = 0.5, 1, 2, 5$ MHz/μs, respectively. The simulation results of readout spectral hole are presented in Fig. 4.

From Fig. 4, it can be seen that if the chirp rate is slower than the square of the homogeneous linewidth, the signal can be read normally and their slight distortion can be ignored. As soon as the chirp rate exceeds the square of the homogeneous linewidth, the readout will exhibit asymmetric, oscillatory, and broadening behaviors, and the resolution is lost, which arises from the dispersion of crystal and read chirped laser. Fortunately, the distorted chirp readout, which arises from the faster chirp rate, can be recovered by post processing, as proposed by Chang *et al.*[13] The results conform with Maxwell–Bloch mode.[14]

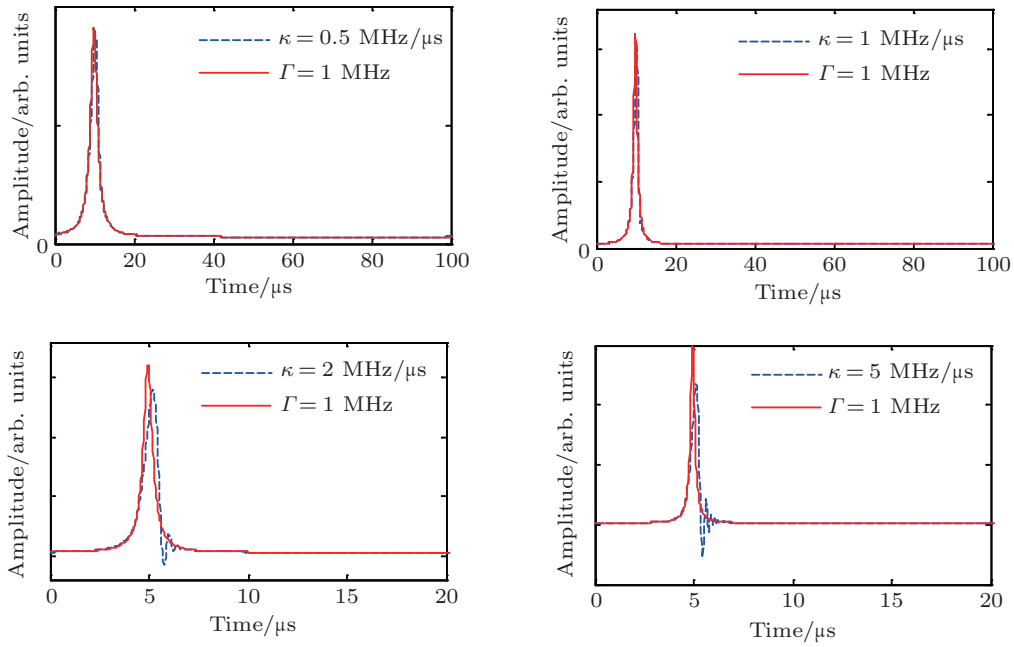


Fig. 4. (color online) Readouts of a single spectral hole using chirped field with chirp rates varying from $\kappa = 0.5$ MHz/μs to $\kappa =$ 5 MHz/μs. The spectral hole has a Lorentzian line shape with width $\Gamma = 1$ MHz.

3. Experimental demonstration and results

The experimental setup for the writing/reading process of the spectral-hole analysis in Tm^{3+}:YAG is shown in Fig. 5(a).[15] The signal beam from a stabilized external cavity diode laser (NewFocus6700) burns a hole at the central frequency where the laser was written into the crystal (Tm, 5 at.%) inhomogeneous profile. One frequency-chirped beam from the reading laser, which is controlled by a saw signal produced by AWG (Agilent 33250A), probes the inhomogeneous profile changed by the beam from the writing laser. The other frequency-chirped beam from the reading laser probes the unchanged inhomogeneous profile of the crystal. The two reading beams are combined at the differential detector, the digitizing oscilloscope (Agilent 54833D MSO) then records the spectral-hole.

In the proof-of-concept experiment, the crystal sits within a cryostat at a temperature of 4.26 K (limited by cryogenic equipment) in order to prevent the phonon from the broadening of the transition.[16] The writing laser intensity is fixed to be 2 mW/cm^2 emitting at a vacuum wavelength centered at 793 nm, corresponding to $^3H_6(0)$–$^3H_4(0)$ absorption transition of Tm^{3+} ions. The chirp rate varies from $\kappa = 0.04$ MHz/μs to $\kappa = 4$ MHz/μs. The experimental result of the readout signal at $\kappa = 0.0387$ MHz/μs is shown in Fig. 4(b), and the measured spectral-hole width is 5.36 MHz. At 4.26 K, the homogeneous linewidth of the ions is $\Gamma \approx 1$ MHz. Other measured data of spectral-hole width and spectral-hole depth are shown in Table 1.

As expected, spectral-holes are broader at a higher chirp rate. From Table 1, we can see that the spectral-hole width is basically the same at the lower chirp rate in a range from 0.04 MHz/μs to 0.2 MHz/μs, which is also consistent with the theoretical results. But when the chirp rate range from 0.4 MHz/μs to 4 MHz/μs, the spectral-hole has a serious distortion, which our equipment may own. The value of the spectral-hole width is larger than the homogeneous linewidth of the ions at 4.26 K (2×1 MHz = 2 MHz) because of a variety of parameters including but not restricting the stability of the laser source, the linewidth of laser source, the dynamic range of the detection device, and the optical shot noise.

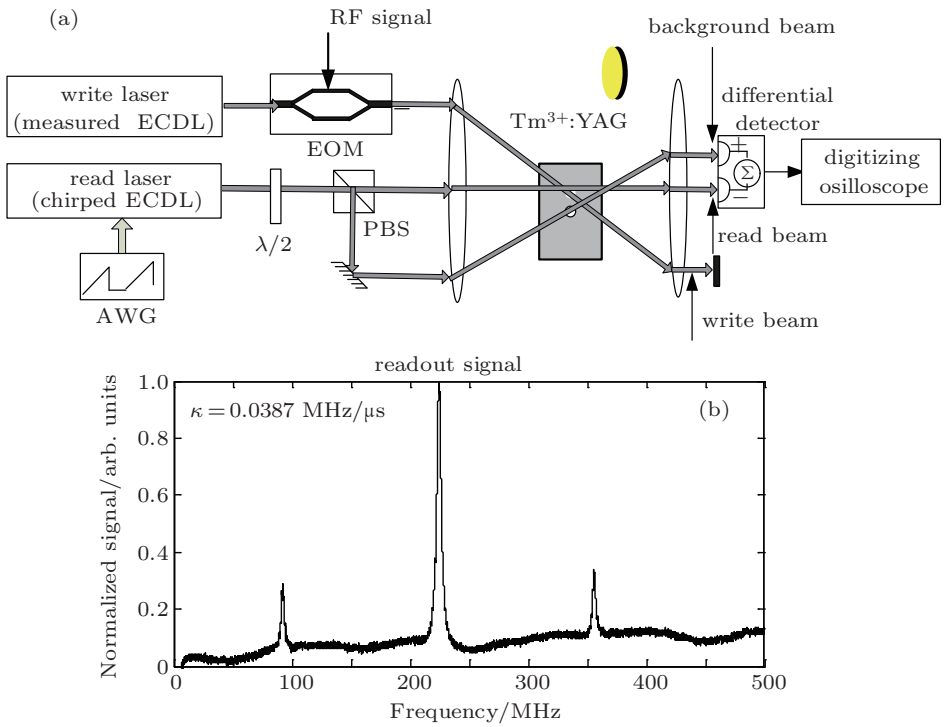


Fig. 5. (color online) Experimental demonstration: (a) writing/reading process for spectral-hole analysis in SHB crystal. AWG stands for arbitrary waveform generator, PBS for polarizing beam splitters, EOM for electro–optic modulator, ECDL for external cavity diode laser; (b) the experimental results of the readout signal.

Table 1. Chirp rate dependences of the measured spectral-hole width and depth.

κ/(MHz/μs)	0.04	0.05	0.08	0.1	0.2	0.4	1	2	4	8
W/MHz	5.38	5.34	6.15	5.73	7.53	10.14	20.30	39.1	73.2	–
D/mV	0.058	0.049	0.057	0.049	0.041	0.03	0.019	0.013	0.002	0.002

4. Conclusions and discussion

In this paper, we bridge the gap between spectral-hole burning and three-pulse photon echo based on perturbation theory. The characteristics of spectral-hole burning based on perturbation theory are analyzed. According to the theoretical results, spectral-hole burning can be explained as a photon echo of the zero-order diffraction echo when the first optical pulse and the second optical pulse are overlapped in time. By using this model, we can solve the problem of interaction between complex pulse and the SHB crystal material. According to the model, the spectral-hole width is dependent on the chirp rate of the reading laser. For a chirped field with $\kappa \ll \Gamma^2$, the spectral hole is closely mapped into the time domain, while for $\kappa > \Gamma^2$ distortions are observed. In the small signal regime, the simulation results conform with the Maxwell–Bloch mode. We also experimentally demonstrate that in Tm^{3+}: YAG within cryogenic temperature the spectral-hole width is dependent on chirp rate of the reading laser. The value of spectral-hole width measured in the experiment is larger than the homogeneous linewidth of the ions because of the contribution of the laser frequency jitter. Our future developments aim to realize a servo-control of the writing laser to control the frequency jitter, which will allow us to obtain a high resolution hole.

References

[1] Guillaume G, Vincent C, Ivan L, Le Gouët J L and Fabien B 2005 *IEEE Photon. Technol. Lett.* **17** 2385

[2] Colice M, Schlottau F and Wagner K H 2006 *Appl. Opt.* **45** 6393

[3] Chaneliere T, Bonarota M, Damon V, Lauro R, Ruggiero J, Lorgeré I and Le Gouët J L 2010 *J. Lumin.* **130** 1572

[4] Simon C, Afzelius M, Appel J Boyer, de la Giroday A, Dewhurst S J, Gisin N, Hu C Y, Jelezko F, Kroll S, Muller J H, Nunn J, Polzik E, Rarity J, de Riedmatten H, Rosenfeld W, Shields A J, Skold N, Stevenson R M, Thew R, Walmsley I, Weber M, Weinfurter H, Wrachtrup J and Young R J 2010 arXiv: 1003.1107v1 [quant-ph]

[5] Damon V, Crozatie R V, Chanelière T, Le Gouët J L and Lorgeré I 2010 *J. Opt. Soc. Am. B* **27** 524

[6] Christoffer J R, Randy R R, Mingzhen T, Chang T J and Babbitt W R 2007 *J. Opt. Soc. Am. B* **24** 2979

[7] Wang W, Ma X R, Chen L, Zhang S G and Zhao J 2012 *Chin. Phys. Lett.* **29** 100601

[8] Li Y Z, Hemmer P, Kim C H, Zhang H L and Wang L H 2008 *Opt. Express* **16** 14862

[9] Mitsunaga M and Brewer R G 1985 *Phys. Rev. A* **32** 1605

[10] Guillot N, Goldner P, Antic F E and Le Gouët J L 2005 *Phys Rev. B* **71** 174409

[11] Meystre P and Sargent M III 2007 *Elements of Quantum Optics*, 4th edn. (New York/Berlin/Heidelberg: Springer) p. 118

[12] Allen L and Eberly J H 1987 *Optical Resonance and Two-level Atoms* (New York, Dover Publications, Inc.)

[13] Chang T J, Tian M Z, Mohan R K, Renner C, Merkel K D and Babbitt W R 2005 *Opt. Lett.* **30** 1129

[14] Chang T J, Mohan R K, Tian M Z, L.Harris T, Babbit W R and Merkel K D 2004 *Phys. Rev. A* **70** 063803

[15] Chen L, Ma X R, Wang W, Zhang S G, Mu K L, Wang X Y and Zhang S Y 2013 *Chin. Phys. B* **22** 064213

[16] Deng H X, Jiang X D, Xiang X, Sun K, Yuan X D, Zheng W G, Gao F and Zu X T 2010 *Chin. Phys. B* **19** 107801